Evolution of the Curie temperature for a substituted Cantor alloy

Jakub Šebesta [1,2,3] Karel Carva [1] and Dominik Legut [2,3,*]

[1]*Department of Condensed Matter Physics, Faculty of Mathematics and Physics, Charles University, Ke Karlovu 5 121 16 Praha 2, Czech Republic*

[2]*IT4Innovations, VSB-Technical University of Ostrava, 17 listopadu 2172/15, 708 00 Ostrava-Poruba, Czech Republic*

[3]*Nanotechnology Centre, CEET, VSB-Technical University of Ostrava, 17 listopadu 2172/15, 708 00 Ostrava-Poruba, Czech Republic*

(Received 11 August 2020; revised 8 December 2020; accepted 13 January 2021; published 4 February 2021)

Knowledge of the magnetic ordering temperature is one of the fundamental physical properties characterizing material behavior. Magnetism is not only related to the magnitude of magnetic moments within specific magnetic ordering, but it also influences other physical properties. In the present work, we determine magnetic ordering temperatures for high-entropy alloys (HEAs), with examples of the Al- and Mo-based Cantor alloy derivatives. Nowadays, HEAs represent a promising class of materials in the sense of mechanical engineering. Regarding the paramagnetic state of the well-known and well-explored Cantor alloy, we deal with its Mo and Al derivatives, which offer higher possible ordering temperatures. We discuss the differences between *p*-type and *d*-type substitution as well as their influence on the magnetic behavior. We determine the ordering temperatures based on the *ab initio* calculated magnetic exchange interactions in terms of the mean-field approximation, random-phase approximation, and Monte Carlo simulations. Based on the thorough description of magnetic pair exchange interactions, a particular composition's influence on the achieved critical temperatures is described.

DOI: 10.1103/PhysRevB.103.064407

I. INTRODUCTION

High-entropy alloys (HEAs) are well known and well studied thanks to their unique physical properties, ensuring their high application potential, especially their mechanical properties [1–3]. HEAs are based on multiple principal elements. This allows for a large entropy contribution that stabilizes them. It differentiates them from classical alloys, and it provides a great variability of their properties [3,4]. Regarding applications, magnetic behavior [4,5] is significant, despite being far less studied. One should recognize that it not only determines the temperature range of the alloy in different magnetic states, i.e., magnetic ordering temperature, but it also influences phase stability, crystal structure [6,7], and mechanical properties [8,9].

In this work, we focus on the magnetic ordering and exchange interactions of the prototype CrMnFeCoNi HEA based on magnetic 3*d* elements, the so-called Cantor alloy [10], in the presence of nonmagnetic substitutions. Despite being composed of magnetic elements, this alloy is paramagnetic under ambient conditions [11] as it bears only weak magnetic moment per site. Some experiments suggest just spin-glass behavior at quite low temperature [12]. It is supposed to originate in the frustration of magnetic moments as complex magnetic exchange interactions occurring among magnetic 3*d* metals [13–15]. However, it has been demonstrated that appropriate substitution can bring a modification of the crystal structure [16,17], which is highly responsible for the character of pair exchange interactions [14,18], and that a substitution is able to suppress the interplay of ferromagnetic (FM) and antiferromagnetic (AFM) elements, which reduces magnetic moments magnitudes [14]. Therefore, by using a suitable substitution, it is possible to enhance substantially critical temperatures. Experiments and theoretical calculations show that they can considerably exceed the room temperature [16,18–20], which gives them potential to be used in industrial applications.

We focus on the impact of the type and the position of the substitution on the magnitude of achievable critical temperatures, concerning a possible generalization of the observed behavior, which might be useful for designing materials based on CrMnFeCoNi with a high critical temperature. To cover a wider range of alloys, we deal with a nonmagnetic *d*-metal substitution as well as a *p*-metal one. Our choice of Mo-based alloys [14] and Al-based ones, where the magnetism has been partially discussed in the literature [16–18], is motivated by our further insights [14]. Besides the strength of the magnetism as a function of the form of the substitution, we discuss the character of the magnetic pair exchange interactions as well as the reliability of the employed approaches used for the evaluation of critical temperatures.

This paper is organized as follows. Section II describes the methods employed to evaluate magnetic exchange interactions and ordering temperatures. In Sec. III general trends of calculated exchange interactions and ordering temperatures depending on the composition are discussed. Finally, the main results of our study are concluded in Sec. IV.

II. FORMALISM

Evaluation of critical temperatures T_C of Al- and Mo-based Cantor alloy derivatives is based on quantum-mechanical electronic structure calculations. They rely on the tight-binding linear muffin-tin method (TB-LMTO) employing the

*Corresponding author: dominik.legut@vsb.cz

Green's function (GF) formalism within the atomic sphere approximation [21,22], where the fully relativistic (FR) treatment is employed. Our previous calculations [14] showed that it is needed to achieve reliable results as the scalar relativistic treatment provides suppressed magnetic behavior. The exchange-correlation potential is described by the local spin density approximation and the potential of Vosko *et al.* [23]. An s, p, d atomic model is involved.

The use of TB-LMTO allows treating the disorder in the framework of the coherent potential approximation (CPA) [24]. The CPA is a highly efficient method to solve small unit cells and small perturbations. Hence, it suits alloys composed of rather similar atoms or alloys near equimolar composition, which are well disordered. The CPA neglects the local environment effects, including local distorting. Therefore, a homogeneous alloy is simulated. Finally, a basic screened impurity model is involved in improving electrostatics in disordered systems [25]. The elemental cell is constructed by reflecting the element metallic radii [26]. Although the muffin-tin-based methods allow for only a simple relaxation, they provide reliable observations, as shown recently in papers where HEAs were successfully solved [14,18,27,28].

The TB-LMTO method based on GFs allows one to compute magnetic pair exchange interactions J_{ij} employing the magnetic force theorem [29,30]. Furthermore, the vertex cancellation theorem ensures the validity in the presence of disorder involving the conditionally averaged Green's function [31]. Concerning the effective Heisenberg Hamiltonian [Eq. (1)] [30] the pair exchange interaction $J_{ij}^{\alpha\beta}$ describes the magnetic exchange interaction between atoms of the α and β types occupying sites $\mathbf{R}_i$ and $\mathbf{R}_j$, respectively.

$$\mathcal{H}_{\mathrm{ex}} = -\sum_{ij} J_{ij}^{\alpha\beta}(\mathbf{R}_i - \mathbf{R}_j)\, \mathbf{e}_i(\mathbf{R}_i) \cdot \mathbf{e}_j(\mathbf{R}_j). \tag{1}$$

In the framework of the CPA Liechtenstein's formula [29,30,32] for the conditionally averaged pair exchange interaction reads

$$\bar{J}_{ij}^{\alpha\beta} = \frac{1}{4\pi}\mathrm{Im}\int_C \mathrm{Tr}_{\mathrm{L}}\big[\Delta_i^{\alpha}(z)\, \bar{g}_{ij}^{\alpha\beta,\uparrow}(z)\, \Delta_j^{\beta}(z)\, \bar{g}_{ji}^{\beta\alpha,\downarrow}(z)\big]dz. \tag{2}$$

The energy integration is performed along the contour C in the upper part of the complex plane involving the occupied part of the valence band. Tr_{L} stands for the trace over the angular momentum indices $L = (l, m)$. $\Delta_i^{\alpha}(z)$ describes the spin splitting of the LMTO potential function, and $\bar{g}_{ij}^{\alpha\beta,\sigma}$ represents the spin-resolved part of the conditionally averaged Green's function. In the present work, $J_{ij}^{\alpha\beta}$'s are evaluated by employing outcomes from FR electronic structure calculations.

Within the CPA, the simulated system is well disordered, and the translation symmetry is maintained. Pair exchange interactions depend only on the position of the atomic sites within the elemental cell, their occupation, and the pair distance $|\mathbf{R}_i - \mathbf{R}_j|$. This approach allows one to evaluate the on-site average pair exchange interaction $\bar{J}_i^{0,\alpha}$ by a simple summation over all neighboring atomic shells [30] as follows:

$$\bar{J}_i^{0,\alpha} = \sum_{\beta}\sum_{j} \bar{J}_{ij}^{\alpha\beta} c_j^{\beta}, \tag{3}$$

where the concentration c_j^{β} of the counterpart of the β type is considered. The infinite summation can be avoided [32]. The effective on-site exchange interaction over the whole crystal can be obtained directly by conditionally averaged Green's functions $\bar{g}^{\alpha,\sigma}(z)$. It yields

$$\bar{J}_i^{0,\alpha} = -\frac{1}{4\pi}\mathrm{Im}\int_C \mathrm{Tr}_{\mathrm{L}}\big\{\Delta_i^{\alpha}(z)\big[\bar{g}_{ii}^{\alpha,\uparrow}(z) - \bar{g}_{ii}^{\alpha,\downarrow}(z)\big] + \big[\Delta_i^{\alpha}(z)\, \bar{g}_{ii}^{\alpha,\uparrow}(z)\, \Delta_i^{\alpha}(z)\, \bar{g}_{ii}^{\alpha,\downarrow}(z)\big]\big\}dz. \tag{4}$$

The knowledge of the effective on-site interaction possibly allows one to determine the critical temperature T_{C} by means of the mean-field approximation (MFA). The MFA is the simplest approximation, which neglects spin correlation and is valid only in the high-temperature limit. Therefore, it yields overestimated critical temperatures [30,32–35]. However, it serves as a useful upper limit for the T_{C},

$$k_{\mathrm{B}} T_{\mathrm{C}}^{\mathrm{MFA}} = \tfrac{2}{3} J^0. \tag{5}$$

Concerning a random alloy, one has to tackle the dependence of the effective exchange interaction $J^{0,\alpha}$ on the selected element α. The simplest solution, which neglects the disorder in principle, is the so-called average lattice model (ALM) [32,34,36]. It leads to averaging $J^{0,\alpha}$ and straightforward application of Eq. (5).

However, the appropriate way to estimate T_{C} of a multisublattice system in the framework of the MFA is to solve the eigenvalue problem of the symmetric matrix $\mathbb{J}(\mathbf{0})$ [30,35], defined as

$$\mathbb{J}^{\alpha\beta}(\mathbf{q}) = c^{\beta} \sum_i \bar{J}_{0i}^{\alpha\beta} \exp(\mathrm{i}\,\mathbf{q} \cdot \mathbf{R}_i). \tag{6}$$

Then, the corresponding critical temperature $T_{\mathrm{C}}^{\mathrm{MFA}}$ is related to the maximal eigenvalue $j_{\max}$ of the matrix $\mathbb{J}(\mathbf{0})$. It yields

$$k_{\mathrm{B}} T_{\mathrm{C}}^{\mathrm{MFA}} = \tfrac{2}{3} j_{\max}. \tag{7}$$

The random-phase approximation (RPA) represents an improvement of the MFA [33–35,37]. It allows for the existence of magnons, and therefore, it describes more accurately the behavior in the vicinity of T_{C}. Regardless of the type of the magnetic order (ferromagnetic, ferrimagnetic, etc.) the RPA suppresses the value of the critical temperature in comparison to the MFA ($T_{\mathrm{C}}^{\mathrm{RPA}} < T_{\mathrm{C}}^{\mathrm{MFA}}$) [35]. For a simple lattice the critical temperature obeys the following relation:

$$\frac{1}{k_{\mathrm{B}} T_{\mathrm{C}}^{\mathrm{RPA}}} = \frac{3}{2}\frac{1}{N}\sum_{\mathbf{q}} [J^0 - J(\mathbf{q})]^{-1}. \tag{8}$$

The case of a multisublattice system is described in Sec. A 1.

One of the most reliable methods to obtain the critical temperature of a system described by the effective Heisenberg Hamiltonian [Eq. (1)] is the method of Monte Carlo simulations (MC) [38–40]. We utilize the Metropolis algorithm implemented in the Uppsala Atomistic Spin Dynamics (UPPASD) package [41,42]. The temperature dependence of the magnetization $M(T)$ is obtained by the so-called simulated annealing technique, where a system heated up at a temperature substantially higher than the critical temperature T_{C} is slowly cooled down. Each temperature point consists of about 10^5 MC steps in our simulations. For more details, we refer to Sec. A 2.

TABLE I. Calculated magnitudes of magnetic moments of Al-based derivatives depending on the crystal structure and magnetic phase. Total energy differences are stated for comparison.

Alloy	Lattice / Magnetic structure	$E_{\mathrm{fcc-bcc}}$ (mRy)	$E_{\mathrm{DLM-FM}}$ (mRy)	fcc: Magnetic moments per element (in units of μ_B)					Average	$E_{\mathrm{DLM-FM}}$ (mRy)	bcc: Magnetic moments per element (in units of μ_B)					Average
AlMnFeCoNi	FM	3.41		−0.03	−1.53	1.85	0.72	0.12	0.22		−0.09	2.04	2.23	1.44	0.44	1.21
	DLM	0.07	0.27	0.00	−1.78	1.69	0.00	0.00	−0.02	3.62	0.00	2.03	2.08	0.85	0.00	0.99
CrAlFeCoNi	FM	3.36		−0.43	−0.04	1.77	0.73	0.15	0.43		−0.09	−0.06	2.08	1.23	0.20	0.67
	DLM	1.77	0.52	0.00	0.00	1.51	0.00	0.00	0.30	2.10	0.00	0.00	1.94	0.70	0.00	0.53
CrMnAlCoNi	FM	3.24		−0.29	0.97	−0.01	0.17	0.04	0.18		−0.23	1.43	−0.04	1.13	0.16	0.49
	DLM	2.35	−0.15	0.00	1.39	0.00	0.00	0.00	0.28	0.75	0.00	−1.08	0.00	−0.73	0.00	0.36
CrMnFeAlNi	FM	5.35		−0.01	−0.89	1.43	−0.01	0.04	0.11		−0.33	0.96	1.92	−0.05	0.21	0.54
	DLM	4.39	0.05	0.00	1.19	1.31	0.00	0.00	0.50	1.01	0.00	0.00	1.77	0.00	0.00	0.35
CrMnFeCoAl	FM	6.74		−0.11	−0.42	1.23	0.17	−0.01	0.17		−0.28	1.23	1.97	1.30	−0.07	0.83
	DLM	3.91	0.08	0.00	−0.65	1.12	0.00	0.00	0.09	2.90	0.00	0.00	1.84	0.82	0.00	0.53

III. RESULTS AND DISCUSSION

In our recent work [14], we tried to describe magnetic behavior in the well-known Cantor alloy [10] based on the Mo substitution, which leads to the crystal structure transformation and enhancement of the ground state magnetism [14], which promises relatively high ordering temperatures. We found that the bcc structure exhibits a high density of states at the Fermi level [14] in the nonmagnetic state, which usually governs strong magnetic interactions [14,18] in the case of a spin-polarized state. Nonetheless, the ground state bcc crystal structure seems to be unstable at ambient temperatures in the case of Mo-based derivatives [43–45]. Therefore, Al-based derivatives seem to be advantageous as they tend toward bcc crystal structure based on recent experiments [16,46–50].

Having calculated the magnetic ground state properties of Al-based alloys, one can find that they follow the behavior of the Mo ones (compare results in Table I with those of Ref. [14]). Naturally, a preference for the bcc crystal structure, which has stronger magnetism than the fcc one according to previous studies [14,18], and a tendency towards an FM structure are observed. In addition, the substitution of AFM elements still leads to the enhancement of the magnetic moments (Table I). One should be aware of increased magnetic moment magnitudes in comparison to the former Mo derivatives. The increase originates from slightly larger Al metallic radii as well as missing hybridization with d states [51] of the nonmagnetic substitution. It is evident for both considered crystal structures (Fig. 1). Concerning the fcc crystal structure, the missing hybridization causes a shifting of d states towards the Fermi level, enhancing the magnetic moment. Regarding the bcc counterpart, the density of states (DOS) is more complicated due to the occurrence of d-state splitting, apparently caused by a cubic crystal field. Assuming octahedral crystal field splitting, the e_g states are placed near the Fermi level E_F as they are higher in energy than the t_{2g} ones. Not only does the presence of these narrow d states at E_F enhance the magnitudes of the magnetic moments in comparison to the fcc crystal structure, but also it makes bcc structures sensitive to the actual composition as more substantial average magnetic moment changes occur with the p or d nonmagnetic substitution. Concerning the missing hybridization, the p substitution brings about both relative suppression of magnetic moments in comparison to the Mo counterparts in the case of substituted Co and Ni and their relative enhancement when Cr or Fe is replaced.

Although the energy differences between FM and paramagnetic states, described by disordered local moments (DLMs), are rather reduced compared to Mo derivatives (Table I vs results in Ref. [14]), the ordered FM state prevails over DLMs in almost all cases. In addition, magnetic properties in the presence of either p or d substitution hardly change. Therefore, thanks to the higher stability of the bcc phase at higher temperatures with respect to Mo derivatives, the Al-based counterparts are more suitable candidates.

A. Pair exchange interactions

Having calculated the electronic structure, for details concerning Mo derivatives, we refer the reader to Ref. [14]; we evaluate the appropriate pair exchange interactions employing Liechtenstein's formula [Eq. (2)] up to a distance of $9a$, where a is the lattice parameter. A sufficiently high number of neighboring atomic shells is crucial for reliable estimation of critical temperatures T_C. However, one can observe that the exchange interactions rapidly decay (Fig. 2), which promises rather good convergence with the number of included neighbors.

In addition, we point out that the exchange interactions' calculations focus not only on the FM phase but also on the paramagnetic phase described by a DLM state. Strictly speaking, the FM and DLM states stand for the limiting cases of the magnetic order. One describes a perfectly ordered system; the other one describes an absolute disorder. Therefore, both approaches are employed to grasp a more realistic description. Finally, we note that we neglect the breaking of the cubic symmetry of exchange interactions by the spin-orbit coupling. It causes only weak perturbation of J_{ij} magnitudes. Namely, it changes T_C^{MFA} less than about 0.1 K.

B. Mean-field approximation

The most straightforward evaluation of the critical temperature T_C relies on the MFA. Based on the calculated exchange

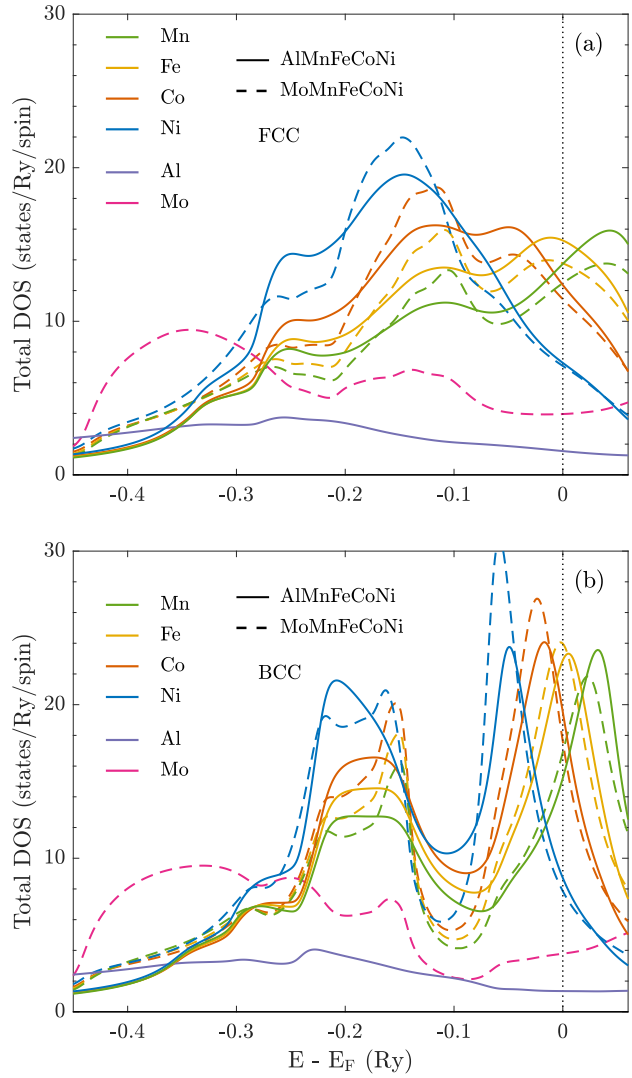

FIG. 1. Comparison of DOSs related to Al and Mo substitutions in a nonmagnetic *X*MnFeCoNi alloy.

interactions $J_{ij}^{\alpha\beta}$, we estimate the critical temperatures T_C^{MFA} according to the eigenvalues of matrices $\mathbb{J}^{\alpha\beta}(\mathbf{0})$ [Eqs. (6) and (7)]. Over 100 atomic shells is sufficient to achieve convergence better than 0.1 K (Fig. 3). In addition, it is evident that T_C's of the Al derivatives converge faster than those of the Mo counterpart. The faster convergence is generally valid due to the weaker exchange interactions in the case of Al derivatives (Fig. 2). Therefore, a smaller number of neighboring shells is possibly needed there. Finally, we note that we do not restrict ourselves to the bcc crystal structures possessing stronger magnetism (Tables II and III), and we also include the fcc structure (Appendix B, Tables IV and V) for comparison. It explains well the contrast between both crystal structures concerned.

In addition, the most straightforward way to estimate T_C within the framework of the MFA could be directly with the mean value of the average on-site exchange interaction $\bar{J}_i^{0,\alpha}$ obtained by Eq. (3) or Eq. (4), based on the ALM. Nevertheless, it neglects the randomness of the alloy and leads to underestimated critical temperatures $T_C^{\mathrm{MFA-ALM}}$ compared to the previous approach. In general, the ALM is more common to describe the behavior of an alloy containing diluted magnetic atoms [32]. We note that the DLM state is simulated in the CPA by employing merely two opposite spins on single atomic sites. Regarding the ALM case, employing both spin sublattices would lead to zero critical temperatures. Thus, we restrict our study to only on one of them, seeking magnetic ordering within the DLM phase, which generally provides distinct critical temperatures. We proceed similarly in the subsequent approaches.

C. Random-phase approximation

Knowing the MFA critical temperatures, we concentrate on an improvement, which resides in the RPA. It is convenient to know T_C^{MFA} before to set a sufficiently high initial temperature based on Eqs. (A1) and (A2). According to the theory, the RPA, which also concerns the spin excitations, yields reduced critical temperatures T_C^{RPA} compared to the MFA. In the case of Al-based derivatives within the bcc structure, the reduction is generally about 70 K except in the case of substituted Fe (Table III). This value indicates a magnitude similar to the spin correlation. Similar behavior is also observed for bcc Mo-based counterparts. Furthermore, a relative reduction in T_C within the range of 10%–20% corresponds to the ones reported for pure Co or Ni [30]. On the contrary, fcc crystal structures bear more distinct behavior depending on the particular composition. Results show that spin wave excitations are much more important in the case of Mo substitutions (Table IV). The reason is likely their weaker magnetism concerning the fcc structure, and it may indicate higher spin frustration.

D. Monte Carlo simulations

Finally, we evaluate critical temperatures by the Monte Carlo method, which is the most reliable approach. We do not employ such distant pair exchange interactions as in the previous approaches because of high computational demands. Similarly, we also evaluate the critical temperatures T_C^{MC} only for the promising structures based on the previously estimated T_C's. This means we especially avoid the fcc crystals structures.

To estimate T_C^{MC} in the framework of the Binder cumulant $U(L,T)$, supercells of various sizes and with random distributions of constituents are employed. Regarding the FM phase, we used an edge length L of 10 to 25 atoms (Fig. 4). According to the presence of nonmagnetic atoms, the evaluation of the DLM phase requires larger supercells ($L = 20$–30 atoms) to keep a sufficient number of magnetic atoms. Furthermore, we considered the average over five distinct random elements' distributions to include a homogeneous disorder.

In the case of Mo derivatives, we deal with three reduced numbers of neighboring shells N_{sh}, mentioned in Table II, in order to evaluate the influence of the weak convergence of the effective exchange interactions (Fig. 3) on the critical temperature T_C^{MC}. The results show a rather strong dependence of T_C^{MC} on the number of neighboring shells N_{sh}, which almost corresponds to a similar dependence of $T_C^{\mathrm{MFA}}(N_{\mathrm{sh}})$ for appropriate values of N_{sh} (Fig. 3). On the other hand, thanks

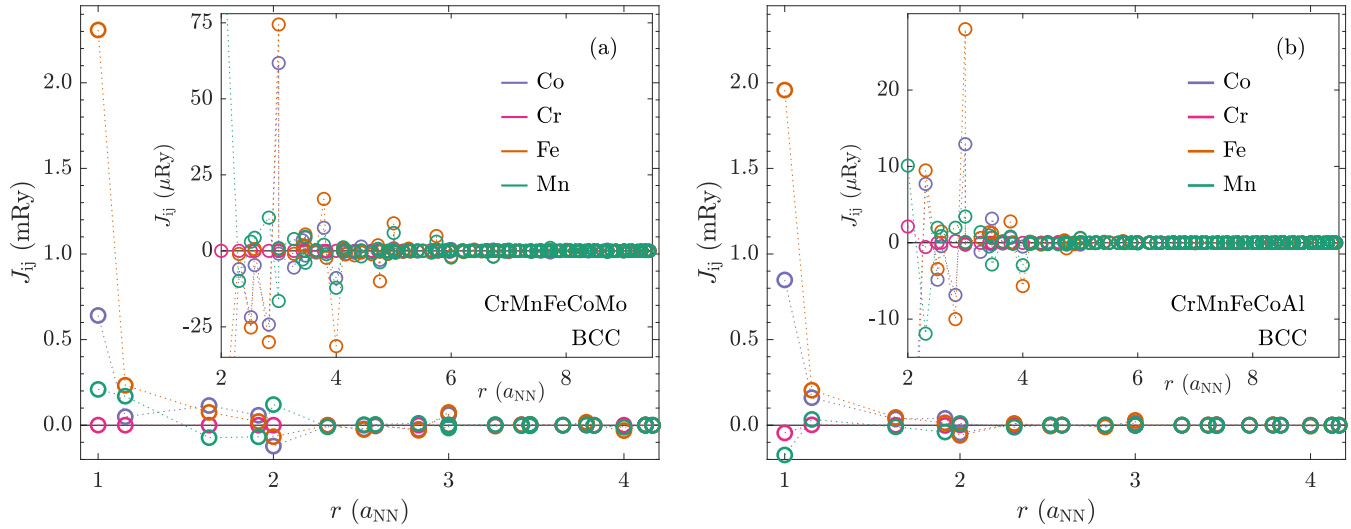

FIG. 2. Distribution of the magnetic pair exchange interactions $J_{ij}^{\alpha\beta}$ as a function of the distance and the type of the element. Only exchange interactions within the sublattice of the same element are depicted. The distance is expressed in units of the nearest-neighbor distance a_{NN}. The FM phase and bcc crystal structure are used. The insets depict exchange interactions' oscillations for larger distances.

to fairly good convergence of Al-based alloys (Fig. 3), only a single shell dimension is used (Table III).

In general, the obtained values of T_C^{MC} are much lower than the critical temperatures obtained not only by the MFA but also by the RPA (Tables II and III). One can suppose an influence of very complex spin correlations, which go beyond the scope of the RPA. Interestingly, the values of T_C^{MC} approach the values obtained within the MFA-ALM. Strictly speaking, this result does not mean that MFA-AFM is a good description. It provides lower critical temperatures, which disagree with general statements. The MFA should stand for a high-temperature limit. However, the MFA-ALM is suitable for a diluted magnetic alloy. Hence, close values might be related to the fact that no all elements bear strong magnetic behavior (compare Table I and the results in Ref. [14]), which could imply a kind of diluted character.

Having mentioned the diluted behavior, we should also notice Ruderman-Kittel-Kasuya-Yosida (RKKY)-like oscillations in the spatial dependence of $(r/a)^3 J_{ij}$ (Fig. 5), where the factor $(r/a)^3$ stands for scaling of the RKKY interaction. The oscillations are nearly exponentially damped, apparently by the presence of disorder [30]. Oscillations damping supports a rather localized character of the exchange interactions depicted in Fig. 2. Moreover, the comparison of Al and Mo alloys (Fig. 5) reveals enhanced screening of exchange interactions in the case of Al alloys as stronger damping of oscillations is observed. It agrees with previously described behavior of exchange interactions themselves and T_C^{MFA}'s (Figs. 2 and 3). The influence of p substitution and the missing d states might be suggested.

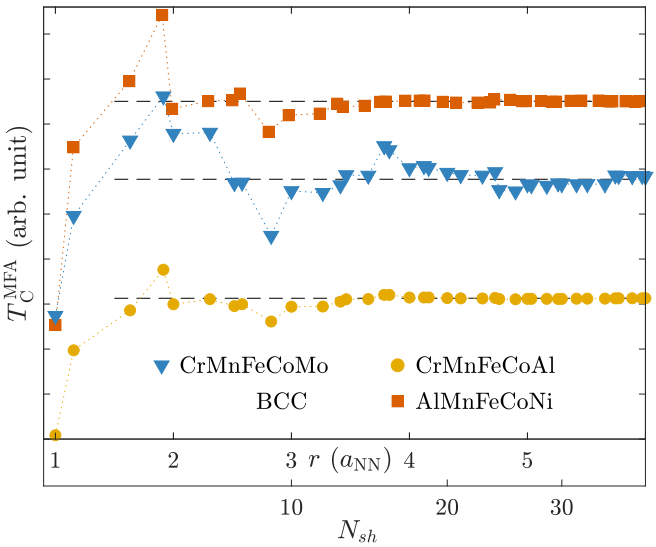

FIG. 3. Dependence of the MFA critical temperature T_C^{MFA} on the number of included atomic shells N_{sh}. The radius of the related sphere of the interacting neighbors in units of nearest-neighbor distance a_{NN} is depicted as well.

E. T_C vs composition and structure

According to our previous studies [14,17,18], we confirm that the type of crystal structure is one of the most important factors which determines the magnitude of the critical temperature regardless of the type of substitution (Tables II and III). A close-packed structure, e.g., the fcc one here, leads to suppression of magnetic exchange interactions overall (Appendix B, Tables IV and V). The present results show that the T_C's in the case of the fcc structure hardly exceed 50 K except for a few Al-based alloys based on the MFA-ALM. These exceptions are related to replacement of AFM elements. It was shown at the beginning of this section that p substitutions lead to stronger magnetic behavior.

On the one hand, in fcc structures, it seems that the presence of several AFM elements indicates an obstacle to the appearance of magnetism [14]. Due to their estimated T_C^{MFA} below the ambient temperature, we do not perform MC simulations for them. On the other hand, bcc structures have about 10 times higher critical temperatures, which corresponds to enhanced exchange interactions or higher magnitudes of

TABLE II. Calculated critical temperatures T_C of Mo-based alloys. The bcc crystal structures are used. MC, Monte Carlo; MFA-ALM, mean-field approximation within the average lattice model; MFA, mean-field approximation of the random alloy; RPA, random-phase approximation of the random alloy; N_{sh}, number of included neighboring shells.

				bcc			
		T_C (K)		T_C (K)			
Alloy	Magnetic phase	N_{sh}	MC	N_{sh}	MFA-ALM	MFA	RPA
CrMnFeCoNi	DLM			70	283	567	495
MoMnFeCoNi	FM	12	420 ± 10	70	478	762	678
		16	470 ± 10				
		23	460 ± 10				
	DLM	23	335 ± 5	70	333	640	558
CrMoFeCoNi	FM	12	270 ± 5	70	249	608	529
		16	320 ± 10				
		23	300 ± 5				
	DLM	23	230 ± 5	70	193	542	462
CrMnMoCoNi	FM			70	0	164	55
	DLM	23	50 ± 15	70	88	226	194
CrMnFeMoNi	FM	12	130 ± 10	70	201	499	415
		16	180 ± 5				
		23	175 ± 5				
	DLM	23	110 ± 15	70	171	532	435
CrMnFeCoMo	FM	12	520 ± 15	70	487	834	746
		16	550 ± 5				
		23	560 ± 5				
	DLM	23	380 ± 10	70	367	690	605

magnetic moments caused by the splitting of *d* states (Fig. 1). We show that both kinds of substituted alloys, either with Mo or Al, can lead to high critical temperatures at the ground state. Nonetheless, based on the experiments [43–45], the Mo-based alloys tend to have an fcc crystal structure at ambient temperatures, which makes them likely less attractive for engineering applications.

We know that the magnetism in studied alloys relies on the iron atoms (Ref. [14] and Table I). Although noticeable Co and Mn magnetic moments occur with substituted iron atoms, negligible T_C^{MC}'s are obtained, which well indicates that the magnetic behavior is rather weak (Tables II and III). Furthermore, one should be aware of the influence of the Co atoms. We showed in our calculations that their absence either leads to a paramagnetic ground state in the case of the Mo substitution [14] or reduces the stability of the FM phase when Co is replaced by Al (Table I) . However, it is relevant to evaluate the strength of the exchange interactions. Naturally, rather weak magnetism yields not very high T_C's. Based on the magnetic moment magnitudes (Table I and Ref. [14]), the most substantial exchange interactions are apparently related to Co, Fe, and Mn. Hence, these elements should be maintained regardless of the *p* or *d* type of the substitution. Unsurprisingly, the critical temperatures scale well with the

TABLE III. Calculated critical temperatures T_C of Al-based alloys. The bcc crystal structures are used. MC, Monte Carlo; MFA-ALM, mean-field approximation within the average lattice model; MFA, mean-field approximation of the random alloy; RPA, random-phase approximation of the random alloy; N_{sh}, number of included neighboring shells.

				bcc			
		T_C (K)		T_C (K)			
Alloy	Magnetic phase	N_{sh}	MC	N_{sh}	MFA-ALM	MFA	RPA
AlMnFeCoNi	FM	25	525 ± 5	50	522	835	756
	DLM	25	370 ± 5	50	315	659	585
CrAlFeCoNi	FM	25	340 ± 5	50	275	634	563
	DLM	25	235 ± 5	50	187	521	451
CrMnAlCoNi	FM	25	75 ± 5	50	121	279	244
	DLM			50	16	58	44
CrMnFeAlNi	FM	25	120 ± 5	50	154	403	338
	DLM	25	45 ± 10	50	77	386	308
CrMnFeCoAl	FM	25	420 ± 5	50	377	678	609
	DLM	25	240 ± 10	50	126	522	453

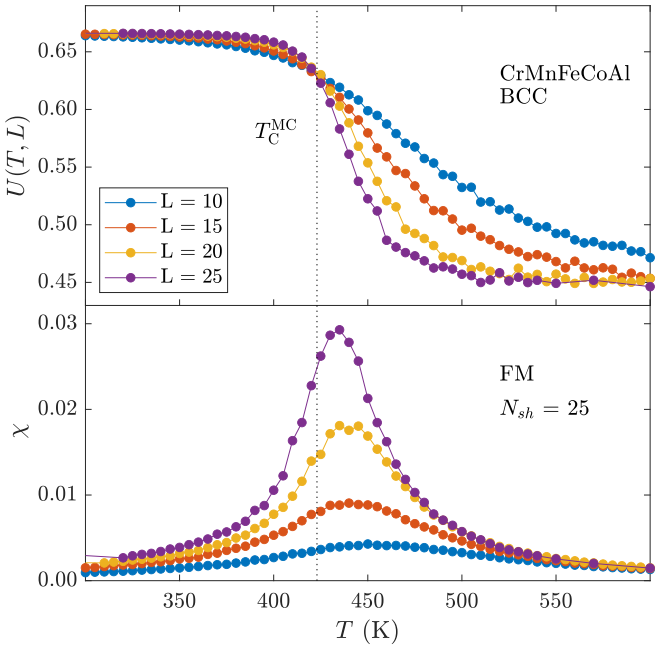

FIG. 4. Evaluation of the Monte Carlo critical temperature T_C^{MC} based on the Binder cumulant curves. The temperature dependence of the magnetic susceptibility χ is depicted for comparison.

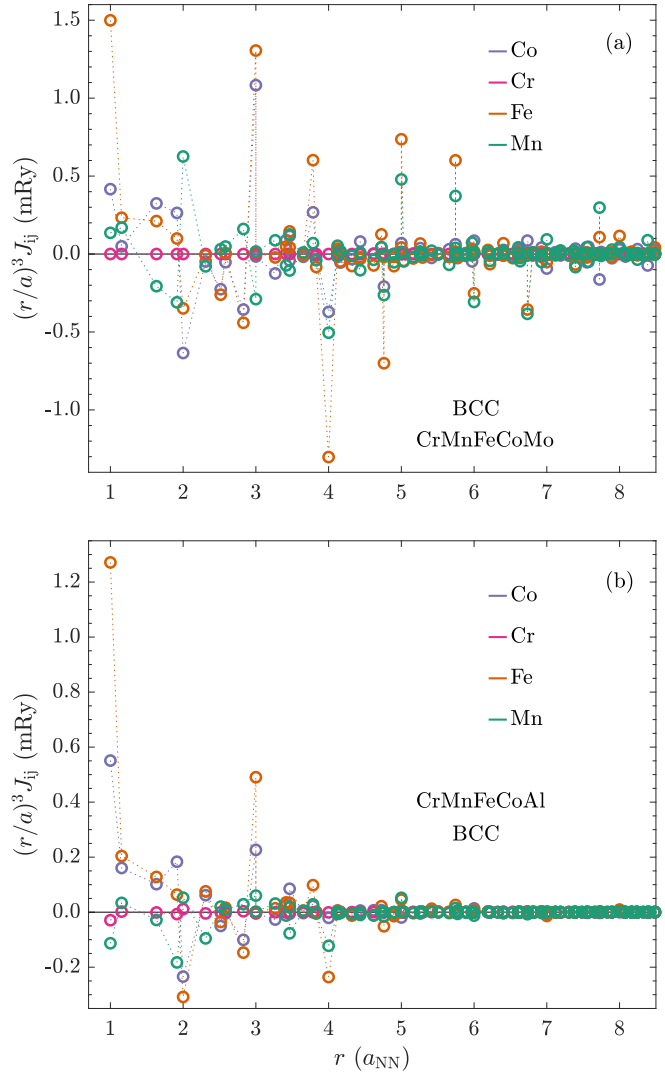

FIG. 5. Damping of long-range RKKY-like oscillations in the radial distribution of pair exchange interactions $J_{ij}^{\alpha\beta}$. The FM phase and bcc crystal structure are used. The distance is expressed in units of the nearest-neighbor distance a_{NN}.

magnitude of the average magnetic moment (Table I and Ref. [14]), and the highest T_C's belong to alloys with substituted Cr or Ni atoms irrespective of nonmagnetic elements. Based on the MC simulation employing bcc crystal structures within the FM phase, critical temperatures overcome 400 K there. Regarding DOSs of nonmagnetic alloys [Figs. 1(b) and 9], Cr and Ni states give the smallest contribution at the Fermi level E_F. Thus, their substitution likely shows the most suitable way to enhance the spin splitting and the magnetic ordering temperature (Fig. 6). This observation corresponds to Curie temperature behavior, as shown in preceding works [9,18].

Concerning experimental results, one can guess that using heavier p-metal atoms might lead to higher T_C [19,20,52]. The increase corresponds to the observed preference of magnetism in more spatial crystal structures. Finally, one should be aware that theoretical and experimental works point to stabilization of the bcc structure by Cr and Fe, whereas it seems that Co and Ni stabilize the fcc one [53,54].

F. Magnon dispersion and $J(\mathbf{q})$ in the Brillouin zone

Having evaluated critical temperatures, one can compare them with calculated exchange interactions in more detail. We focus on the lattice Fourier transformation of exchange interactions $J^{\alpha\beta}(\mathbf{q}) = \sum J_{0i}^{\alpha\beta} \exp(i\mathbf{q} \cdot \mathbf{R}_i)$ not only because we have employed it within the RPA but especially because it displays well magnitudes of the exchange interaction as well as their character.

We deal with the bcc crystal structure, which provides relevant critical temperatures. For clarity, we select the most substantial exchange interactions $J(\mathbf{q})$ (Figs. 7 and 8). We exclude Cr, and almost all Ni related exchange interactions because of their fragility. We recall the related weak magnetic moments of both Cr and Ni (see Table I and Ref. [14], respectively). Compared to the previously shown behavior of J_{ij} (Fig. 2 and Ref. [14]), we display here nearly the total strength of the exchange interactions as it is illustrated by the convergence of T_C^{MFA} (Fig. 3).

One can notice that if pure Fe interactions exist, they remain the most prominent ones regardless of the substitution type, although they change about 10% of their strength as a function of the substitution position. We mentioned that the presence of Fe or Co is essential to obtain significant critical temperatures (Tables II and III). However, the $J(\mathbf{q})$ dependencies (Figs. 7 and 8) clearly show that additional strong Co-related exchange interactions are highly necessary to achieve high critical temperatures, notably, substantial Fe-Co interactions. Furthermore, both Fe and Co interact with Mn to a large extent as well. These interactions stand for the third- or fourth-strongest ones in the presence of Fe atoms. Therefore, based only on the $J(\mathbf{q})$ dependencies, one could

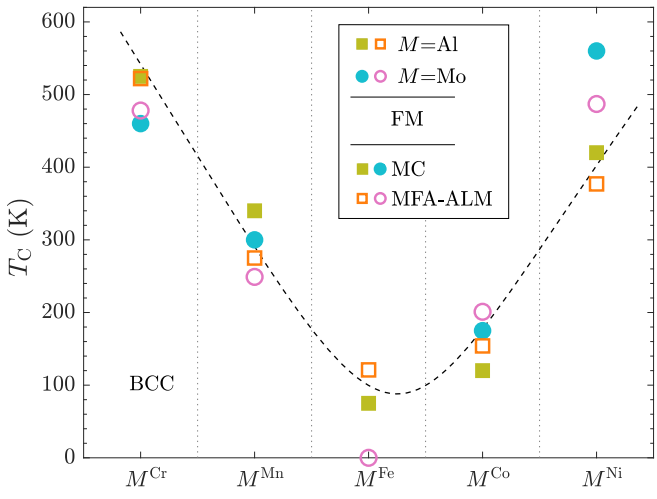

FIG. 6. Comparison of evaluated critical temperatures T_C as a function of the composition and employed approach, where M denotes type of the substitution and the superscript stands for the substituted element. Regarding the Mo-based alloy, $N_{sh} = 23$, and in the case of the Al-based alloys, $N_{sh} = 25$. Solid points depict MC simulations, whereas open ones show the MFA-ALM approach. The dashed curve serves only as an eye guide.

assume that the presence of these three elements is crucial to achieving high T_C, which corresponds to our previous statements.

One can explore particular alloys in detail. In Mo alloys, the highest critical temperature is achieved by the substitution of Ni, which causes enhancement of Fe and Mn related to ferromagnetic exchange interactions. In addition, pure Mn pair interactions, rather, do not reject a ferromagnetic order there. One can notice that only the substitution of either Cr or Ni leads to a set of strong ferromagnetic exchange interactions according to the discussion in the previous section.

Concerning the Al-based counterparts, Mn itself bears fairly strong antiferromagnetic AFM behavior, especially for substituted Cr atoms. However, ferromagnetic exchange interactions are strengthened as well, including also Ni interactions, which brings about the highest T_C there. Generally, the Mn-related interactions are mostly enhanced in the absence of Cr atoms, which indicates a possible frustration of magnetic moments in the presence of both AFM elements [14].

Evaluating the interactions' character, one observes that the pure Mn interactions are almost the only ones that generally repel FM ordering. Especially for Al-based alloys, $J(\mathbf{q})$'s depict a genuine AFM character with maxima at the Brillouin zone boundaries (H points). On the other hand, in the case of Mo-based alloys, the AFM character is not so expressive. However, local maxima of $J(\mathbf{q})$ occur apart from the Γ point. One can observe that $J(\mathbf{q})$ dependencies oscillate much more than the counterparts in the Al derivatives. The reason is most likely the slightly higher importance of spin waves within Mo-based alloys, which follows from the comparison of the related T_C^{MFA} and T_C^{RPA}. In addition, the oscillations might indicate a tendency to a structure more complex than pure FM [14].

IV. CONCLUSION

In the present work, we evaluated magnetic critical temperatures and thoroughly analyzed exchange interactions of alloys derived from the well-known Cantor alloy by nonmagnetic Mo or Al substitutions, which stand for d- and p-metal substitutions, respectively. We showed that the Al derivatives have magnetic behavior similar to the former Mo ones [14] concerning the relation of the position of the nonmagnetic substitution and observed magnetic behavior. Moreover, magnetism seems to be enhanced, especially for fcc crystal structures, thanks to using different substitutions. Increased magnetism originates from the larger Al radii and almost missing hybridization with d states of the substitution.

Based on the obtained values of the critical temperatures, it seems that the most eligible alloys for real industrial applications are likely those with substituted Ni or Cr sites. They possess critical temperatures T_C sufficiently above room temperature with bcc crystal structure and FM ordering regardless of the substituting element. The analysis of the evaluated pair exchange interactions revealed that the presence of Co, Fe, and Mn, including the related exchange interactions, is highly necessary to achieve high critical temperatures, irrespective of the type of substitution.

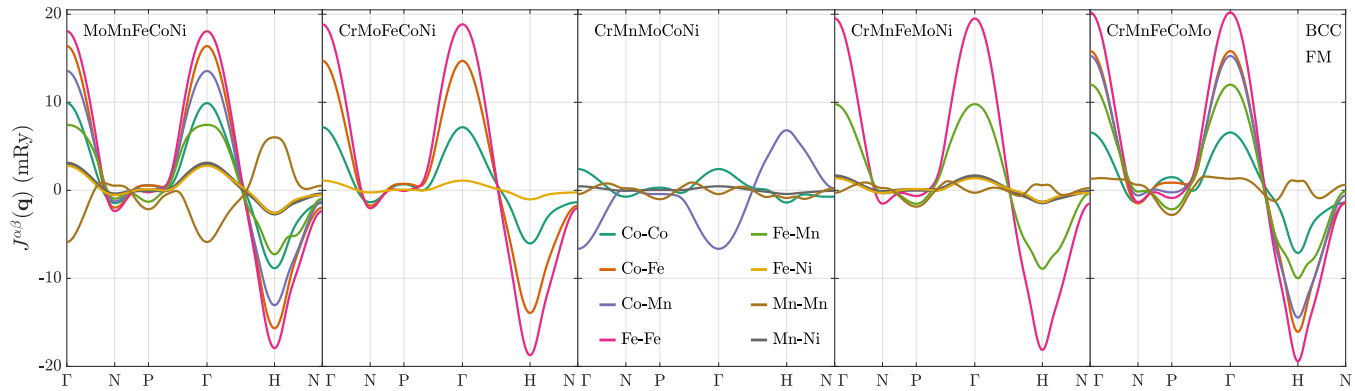

FIG. 7. Mo-based derivatives. Lattice Fourier transformation of the pair exchange interaction along the path in the Brillouin zone. The most substantial interactions within the ferromagnetic phase are depicted.

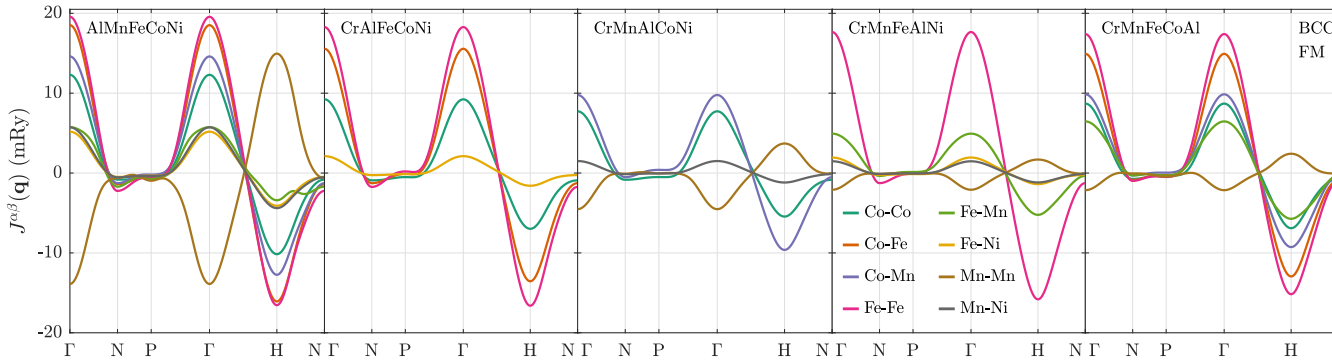

FIG. 8. Al-based derivatives. Lattice Fourier transformation of the pair exchange interaction along the path in the Brillouin zone. The most substantial interactions within the ferromagnetic phase are depicted.

ACKNOWLEDGMENTS

This work was supported by the European Regional Development Fund in the IT4Innovations National Supercomputing Center - Path to Exascale project, Project No. CZ.02.1.01/0.0/0.0/16_013/0001791 within Operational Programme Research, Development and Education and Grants No. 17-23964S (for 2019) and No. 20-18392S (for 2020) of the Czech Science Foundation and European Economic Area grant Project No. EHP-CZ-ICP-1-013, and by the Ministry of Education, Youth and Sports from the Large Infrastructures for Research, Experimental Development, and Innovations project "e-INFRA CZ - LM2018140".

APPENDIX A: CRITICAL TEMPERATURE EVALUATION

1. RPA: Multisublattice systems

Regarding the RPA, the evaluation of the critical temperature in the case of a multisublattice system is more complex as it requires an iterative technique. Self-consistent equations exist which provide the critical temperature T_C^{RPA} [35,37]. Nevertheless, their solution in our case of complicated alloys is not stable enough. Another way to estimate T_C^{RPA}'s is based on a semiclassical approximation of the mean value of magnetic moments [35]. This method is more robust but also more time-consuming. It employs the Langevin function to evaluate the temperature dependence of relative magnitudes of mean values of magnetic moments $\langle e^\alpha \rangle$. The values $\langle e^\alpha \rangle$ obey the relation

$$\langle e^\alpha \rangle = \mathcal{L}\left(\frac{2}{k_B T} \left\{ \frac{1}{\Omega} \int [\mathbb{N}^{-1}(\mathbf{q})]^{\alpha\alpha} d\mathbf{q} \right\} \right), \tag{A1}$$

where T stands for the temperature and the elements of the matrix $\mathbb{N}^{\alpha\beta}(\mathbf{q})$ are defined as follows:

$$\mathbb{N}^{\alpha\beta}(\mathbf{q}) = \delta_{\alpha\beta} \sum_\gamma \mathbb{J}^{\alpha\gamma}(\mathbf{0}) \langle e^\gamma \rangle - \langle e^\alpha \rangle \mathbb{J}^{\alpha\gamma}(\mathbf{q}). \tag{A2}$$

The matrix $\mathbb{J}^{\alpha\beta}(\mathbf{q})$ is composed of the lattice Fourier transformations of the pair exchange interactions $\bar{J}_{ij}^{\alpha\beta}$ [Eq. (6)]. The critical temperature T_C^{RPA} is denoted by the point where the variables $\langle e^\alpha \rangle$ acquire nonzero values. One has to be aware of the divergence, which occurs in Eq. (A1) at $\mathbf{q} = 0$. It can be avoided with an analytical deconvolution [33].

In our calculations, we utilized steps of 1 K above $T = 100$ K; below we reduced the step to about one order of magnitude to keep sufficient sensitivity. In each step, 400 iterations were performed, which is enough to achieve the convergence. The Fourier transformation was performed in the irreducible part of the Brillouin zone consisting of about 44 000 k points (bcc crystal structure).

2. MC simulations and Binder cumulant

In contrast to previously mentioned approaches, the MC method takes into account the spin correlations, which provide exact values of T_C in principle. Furthermore, the MC simulations allow for the disorder (e.g., a random alloy) by using a set of sufficiently large random supercell structures. In reality, the precision of the MC is limited by the inclusion of only a small finite number of the neighboring shells, which neglects long-range magnetic interactions. This limitation stems from the high computational demands of MC simulations.

The most reliable estimation of the critical temperature T_C in the MC simulation framework is the evaluation of the so-called Binder cumulant [55]. It allows for the final size

TABLE IV. Calculated critical temperatures T_C Mo-based alloy. The fcc crystal structure is used. MFA-ALM, mean-field approximation within the average lattice model; MFA, mean-field approximation of the random alloy; RPA, random-phase approximation of the random alloy; N_{sh}, number of included neighboring shells.

Alloy	Magnetic phase	N_{sh}	fcc T_C (K) MFA-ALM	MFA	RPA
MoMnFeCoNi	FM	70	41	71	37
	DLM	70	0	35	14
CrMoFeCoNi	FM	70	47	73	14
	DLM	70	2.0	19	0.3
CrMnMoCoNi	FM	70	0	0	0
	DLM	70	0	0	0
CrMnFeMoNi	FM	70	8.1	21	2.8
	DLM	70	1.8	15	0.3
CrMnFeCoMo	FM	70	6	12	2.7
	DLM	70	1.0	7.8	0.7

TABLE V. Calculated critical temperature T_C Mo-based alloy. The fcc crystal structure is used. MFA-ALM, mean-field approximation within the average lattice model; MFA, mean-field approximation of the random alloy; RPA, random-phase approximation of the random alloy; N_{sh}, number of included neighboring shells.

Alloy	Magnetic phase	N_{sh}	fcc T_C (K) MFA-ALM	MFA	RPA
AlMnFeCoNi	FM	50	64	223	221
	DLM	50	1.2	121	108
CrAlFeCoNi	FM	50	123	217	218
	DLM	50	17	85	76
CrMnAlCoNi	FM	50	0	6	0
	DLM	50	0	0	0
CrMnFeAlNi	FM	50	11	72	67
	DLM	50	0	63	50
CrMnFeCoAl	FM	50	16	44	45
	DLM	50	6.4	34	33

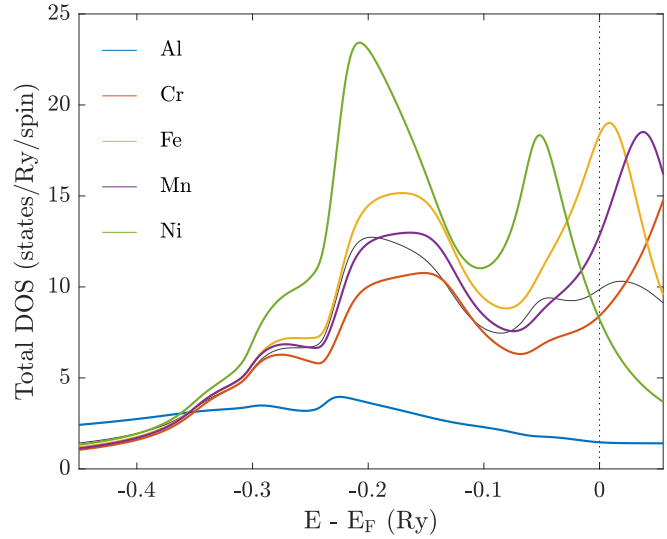

FIG. 9. DOS related to the nonmagnetic CrMnFeAlNi alloy.

effect within the simulated supercell systems. It improves the reliability of the obtained critical temperatures in comparison to common approaches, including the evaluation of the magnetic susceptibility or the specific heat. The Binder cumulant is defined as follows:

$$U \equiv U(L,T) = 1 - \frac{\langle M^4 \rangle}{3\langle M^2 \rangle^2}, \tag{A3}$$

where L denotes the number of elemental cells along one side of the three-dimensional $L \times L \times L$ supercell, $\langle \cdots \rangle$ indicates averaging over MC step at constant temperature T, and M describes the total magnetization of the simulated supercell.

Determination of the critical temperature T_C consists of characteristic critical behavior of the Binder cumulant [55] with respect to T, which reads (i) $\lim_{T\to 0} U(L,T) = \frac{2}{3}$, (ii) $\lim_{T\to\infty} U(L,T) = \frac{1}{L}$, and (iii) $\lim_{T\to T_C} U(L,T) = U^*$. The value U^* stands for an invariant independent of the characteristic size L of the supercell. In addition, it is related to the intersection of the $U(L,T)$ curves obtained for various magnitudes of L, which denotes the critical temperature $T = T_C$ as well.

APPENDIX B: FCC STRUCTURE CURIE TEMPERATURES

To provide a comparison of the studied alloys' magnetic behavior within bcc and fcc crystal structures, we evaluate the critical temperatures for the latter structure type as well (Tables IV and V). We consider both Al- and Mo-based derivatives employing the MFA and RPA framework.

APPENDIX C: LOCAL DOS

For clarity, we append the elements resolved DOS of the another Al-based derivative (Fig. 9). It proves that Cr and Mn states contribution at the Fermi level is minor compared to other 3d elements.

[1] E. J. Pickering and N. G. Jones, High-entropy alloys: A critical assessment of their founding principles and future prospects, Int. Mater. Rev. **61**, 183 (2016).
[2] M.-H. Tsai and J.-W. Yeh, High-entropy alloys: A critical review, Mater. Res. Lett. **2**, 107 (2014).
[3] D. Miracle and O. Senkov, A critical review of high entropy alloys and related concepts, Acta Mater. **122**, 448 (2017).
[4] Y. Ikeda, B. Grabowski, and F. Körmann, Ab initio phase stabilities and mechanical properties of multicomponent alloys: A comprehensive review for high entropy alloys and compositionally complex alloys, Mater. Charact. **147**, 464 (2019).
[5] O. Senkov and C. Woodward, Microstructure and properties of a refractory $NbCrMo_{0.5}Ta_{0.5}TiZr$ alloy, Mater. Sci. Eng., A **529**, 311 (2011).
[6] X. Wu, Z. Li, Z. Rao, Y. Ikeda, B. Dutta, F. Körmann, J. Neugebauer, and D. Raabe, Role of magnetic ordering for the design of quinary twip-trip high entropy alloys, Phys. Rev. Materials **4**, 033601 (2020).
[7] Z. Dong, S. Schönecker, W. Li, D. Chen, and L. Vitos, Thermal spin fluctuations in CoCrFeMnNi high entropy alloy, Sci. Rep. **8**, 12211 (2018).
[8] G. Hausch, Elastic constants of Fe-Pt alloys. I. single crystalline elastic constants of $Fe_{72}Pt_{28}$, J. Phys. Soc. Jpn. **37**, 819 (1974).
[9] H. Ge, H. Song, J. Shen, and F. Tian, Effect of alloying on the thermal-elastic properties of 3d high-entropy alloys, Mater. Chem. Phys. **210**, 320 (2018).
[10] B. Cantor, I. Chang, P. Knight, and A. Vincent, Microstructural development in equiatomic multicomponent alloys, Mater. Sci. Eng., A **375–377**, 213 (2004).
[11] P. Yu, L. Zhang, H. Cheng, H. Zhang, M. Ma, Y. Li, G. Li, P. Liaw, and R. Liu, The high-entropy alloys with high hardness

and soft magnetic property prepared by mechanical alloying and high-pressure sintering, Intermetallics **70**, 82 (2016).

[12] K. Jin, B. C. Sales, G. M. Stocks, G. D. Samolyuk, M. Daene, W. J. Weber, Y. Zhang, and H. Bei, Tailoring the physical properties of Ni-based single-phase equiatomic alloys by modifying the chemical complexity, Sci. Rep. **6**, 20159 (2016).

[13] O. Schneeweiss, M. Friák, M. Dudová, D. Holec, M. Šob, D. Kriegner, V. Holý, P. Beran, E. P. George, J. Neugebauer, and A. Dlouhý, Magnetic properties of the CrMnFeCoNi high-entropy alloy, Phys. Rev. B **96**, 014437 (2017).

[14] J. Šebesta, K. Carva, and D. Legut, Role of magnetism in the stability of the high-entropy alloy CoCrFeMnNi and its derivatives, Phys. Rev. Materials **3**, 124410 (2019).

[15] C. Niu, A. J. Zaddach, A. A. Oni, X. Sang, J. W. Hurt, J. M. LeBeau, C. C. Koch, and D. L. Irving, Spin-driven ordering of Cr in the equiatomic high entropy alloy NiFeCrCo, Appl. Phys. Lett. **106**, 161906 (2015).

[16] Y.-F. Kao, S.-K. Chen, T.-J. Chen, P.-C. Chu, J.-W. Yeh, and S.-J. Lin, Electrical, magnetic, and Hall properties of Al_xCoCrFeNi high-entropy alloys, J. Alloys Compd. **509**, 1607 (2011).

[17] S. Huang, W. Li, X. Li, S. Schönecker, L. Bergqvist, E. Holmström, L. K. Varga, and L. Vitos, Mechanism of magnetic transition in FeCrCoNi-based high entropy alloys, Mater. Des. **103**, 71 (2016).

[18] S. Huang, E. Holmström, O. Eriksson, and L. Vitos, Mapping the magnetic transition temperatures for medium- and high-entropy alloys, Intermetallics **95**, 80 (2018).

[19] S. Huang, A. Vida, D. Molnár, K. Kádas, L. K. Varga, E. Holmström, and L. Vitos, Phase stability and magnetic behavior of FeCrCoNiGe high-entropy alloy, Appl. Phys. Lett. **107**, 251906 (2015).

[20] S. Huang, A. Vida, W. Li, D. Molnár, S. K. Kwon, E. Holmström, B. Varga, L. Károly Varga, and L. Vitos, Thermal expansion in FeCrCoNiGa high-entropy alloy from theory and experiment, Appl. Phys. Lett. **110**, 241902 (2017).

[21] H. L. Skriver, *The LMTO Method: Muffin-Tin Orbitals and Electronic Structure* (Springer, Berlin, 2012).

[22] I. Turek, V. Drchal, J. Kudrnovsky, M. Sob, and P. Weinberger, *Electronic Structure of Disordered Alloys, Surfaces and Interfaces* (Kluwer, Boston, 1997).

[23] S. H. Vosko, L. Wilk, and M. Nusair, Accurate spin-dependent electron liquid correlation energies for local spin density calculations: A critical analysis, Can. J. Phys. **58**, 1200 (1980).

[24] B. Velický, S. Kirkpatrick, and H. Ehrenreich, Single-site approximations in the electronic theory of simple binary alloys, Phys. Rev. **175**, 747 (1968).

[25] P. A. Korzhavyi, A. V. Ruban, I. A. Abrikosov, and H. L. Skriver, Madelung energy for random metallic alloys in the coherent potential approximation, Phys. Rev. B **51**, 5773 (1995).

[26] N. Greenwood and A. Earnshaw, in *Chemistry of the Elements*, 2nd ed., edited by N. Greenwood and A. Earnshaw (Butterworth-Heinemann, Oxford, 1997).

[27] J. Kudrnovský, V. Drchal, F. Máca, I. Turek, and S. Khmelevskyi, Electron transport in high-entropy alloys: Al_xCrFeCoNi as a case study, Phys. Rev. B **100**, 014441 (2019).

[28] F. Tian, L. K. Varga, N. Chen, L. Delczeg, and L. Vitos, Ab initio investigation of high-entropy alloys of 3*d* elements, Phys. Rev. B **87**, 075144 (2013).

[29] A. Liechtenstein, M. Katsnelson, V. Antropov, and V. Gubanov, Local spin density functional approach to the theory of exchange interactions in ferromagnetic metals and alloys, J. Magn. Magn. Mater. **67**, 65 (1987).

[30] I. Turek, J. Kudrnovský, V. Drchal, and P. Bruno, Exchange interactions, spin waves, and transition temperatures in itinerant magnets, Philos. Mag. **86**, 1713 (2006).

[31] P. Bruno, J. Kudrnovský, V. Drchal, and I. Turek, Interlayer Exchange Coupling: The Effect of Substitutional Disorder, Phys. Rev. Lett. **76**, 4254 (1996).

[32] J. Kudrnovský, I. Turek, V. Drchal, F. Máca, P. Weinberger, and P. Bruno, Exchange interactions in III-V and group-IV diluted magnetic semiconductors, Phys. Rev. B **69**, 115208 (2004).

[33] M. Pajda, J. Kudrnovský, I. Turek, V. Drchal, and P. Bruno, Ab initio calculations of exchange interactions, spin-wave stiffness constants, and Curie temperatures of Fe, Co, and Ni, Phys. Rev. B **64**, 174402 (2001).

[34] G. Bouzerar, J. Kudrnovský, L. Bergqvist, and P. Bruno, Ferromagnetism in diluted magnetic semiconductors: A comparison between ab initio mean-field, RPA, and Monte Carlo treatments, Phys. Rev. B **68**, 081203(R) (2003).

[35] J. Rusz, L. Bergqvist, J. Kudrnovský, and I. Turek, Exchange interactions and Curie temperatures in Ni_{2-x}MnSb alloys: First-principles study, Phys. Rev. B **73**, 214412 (2006).

[36] J. Kudrnovský, G. Bouzerar, and I. Turek, Relation of Curie temperature and conductivity: (Ga,Mn)As alloy as a case study, Appl. Phys. Lett. **91**, 102509 (2007).

[37] J. Rusz, I. Turek, and M. Diviš, Random-phase approximation for critical temperatures of collinear magnets with multiple sublattices: GdX compounds (X = Mg, Rh, Ni, Pd), Phys. Rev. B **71**, 174408 (2005).

[38] O. Eriksson, A. Bergman, L. Bergqvist, and J. Hellsvik, *Atomistic Spin Dynamics: Foundations and Applications* (Oxford University Press, Oxford, 2017).

[39] B. Skubic, J. Hellsvik, L. Nordström, and O. Eriksson, A method for atomistic spin dynamics simulations: Implementation and examples, J. Phys.: Condens. Matter **20**, 315203 (2008).

[40] D. Hinzke, U. Atxitia, K. Carva, P. Nieves, O. Chubykalo-Fesenko, P. M. Oppeneer, and U. Nowak, Multiscale modeling of ultrafast element-specific magnetization dynamics of ferromagnetic alloys, Phys. Rev. B **92**, 054412 (2015).

[41] J. Hellsvik, B. Skubic, L. Nordström, B. Sanyal, O. Eriksson, P. Nordblad, and P. Svedlindh, Dynamics of diluted magnetic semiconductors from atomistic spin-dynamics simulations: Mn-doped GaAs, Phys. Rev. B **78**, 144419 (2008).

[42] Uppsala Atomistic Spin Dynamics (UPPASD) code, http://physics.uu.se/uppasd/.

[43] J. W. Bae, J. M. Park, J. Moon, W. M. Choi, B.-J. Lee, and H. S. Kim, Effect of μ-precipitates on the microstructure and mechanical properties of non-equiatomic CoCrFeNiMo medium-entropy alloys, J. Alloys Compd. **781**, 75 (2019).

[44] C. Zhang, B. Liu, Y. Liu, Q. Fang, W. Guo, and H. Yang, Effects of annealing on microstructure and mechanical properties of metastable powder metallurgy $CoCrFeNiMo_{0.2}$ high entropy alloy, Entropy **21**, 448 (2019).

[45] D. Ma, M. Yao, K. Pradeep, C. C. Tasan, H. Springer, and D. Raabe, Phase stability of non-equiatomic CoCrFeMnNi high entropy alloys, Acta Mater. **98**, 288 (2015).

[46] E. Ananiadis, K. Lentzaris, E. Georgatis, C. Mathiou, A. Poulia, and A. E. Karantzalis, AlNiCrFeMn equiatomic high entropy alloy: A further insight in its microstructural evolution, mechanical and surface degradation response, Met. Mater. Int. **26**, 793 (2020).

[47] A. Vallimanalan, S. P. K. Babu, S. Muthukumaran, M. Murali, R. Mahendran, V. Gaurav, and S. Manivannan, Synthesis, characterisation and erosion behavior of AlCoCrMoNi high entropy alloy coating, Mater. Res. Express **6**, 116543 (2019).

[48] A. Karati, K. Guruvidyathri, V. Hariharan, and B. Murty, Thermal stability of AlCoFeMnNi high-entropy alloy, Scr. Mater. **162**, 465 (2019).

[49] K. Guruvidyathri, B. Murty, J. Yeh, and K. H. Kumar, Gibbs energy-composition plots as a tool for high-entropy alloy design, J. Alloys Compd. **768**, 358 (2018).

[50] P. Singh, A. Marshal, A. V. Smirnov, A. Sharma, G. Balasubramanian, K. G. Pradeep, and D. D. Johnson, Tuning phase stability and short-range order through Al doping in $(CoCrFeMn)_{100-x}Al_x$ high-entropy alloys, Phys. Rev. Materials **3**, 075002 (2019).

[51] P. Singh, A. V. Smirnov, and D. D. Johnson, Atomic short-range order and incipient long-range order in high-entropy alloys, Phys. Rev. B **91**, 224204 (2015).

[52] Á. Vida, Z. Maksa, D. Molnár, S. Huang, J. Kovac, L. K. Varga, L. Vitos, and N. Q. Chinh, Evolution of the phase structure after different heat treatments in NiCoFeCrGa high entropy alloy, J. Alloys Compd. **743**, 234 (2018).

[53] M. Ogura, T. Fukushima, R. Zeller, and P. H. Dederichs, Structure of the high-entropy alloy Al_x CrFeCoNi: fcc versus bcc, J. Alloys Compd. **715**, 454 (2017).

[54] B. Ren, Z. Liu, D. Li, L. Shi, B. Cai, and M. Wang, Effect of elemental interaction on microstructure of CuCrFeNiMn high entropy alloy system, J. Alloys Compd. **493**, 148 (2010).

[55] K. Binder, Finite size scaling analysis of Ising model block distribution functions, Z. Phys. B **43**, 119 (1981).